Journal of Physics and Chemistry of Solids 113 (2018) 177–185

Contents lists available at ScienceDirect

Journal of Physics and Chemistry of Solids

journal homepage: www.elsevier.com/locate/jpcs

Synthesis and characterisation of novel low temperature ceramic and its implementation as substrate in dual segment CDRA

Preeti Kumari [a,*], Pankaj Tripathi [a], Bhagirath Sahu [b], S.P. Singh [b], Om Parkash [a], Devendra Kumar [a]

[a] Department of Ceramic Engineering, Indian Institute of Technology (Banaras Hindu University), Varanasi, 221005, India
[b] Department of Electronics Engineering, Indian Institute of Technology (Banaras Hindu University), Varanasi, 221005, India

ARTICLE INFO

Keywords:
Low-temperature co-fired ceramic (LTCC)
Cylindrical dielectric resonator antenna (CDRA)
Sintering temperature
Microstructure

ABSTRACT

Li_2O-(2-3x)MgO-(x)Al_2O_3-P_2O_5 (LMAP) (x = 0.00–0.08) ceramic system was prepared through solid state synthesis route at different sintering temperatures (800–925 °C). A small addition of Al_2O_3 (x = 0.02) in LMAP ceramics lowers the sintering temperature by more than 100 °C with good relative density of 94.13%. The sintered samples were characterized in terms of density, apparent porosity, water absorption, crystal structure, micro-structure and microwave dielectric properties. Silver compatibility test is also performed for its use as electrode material in low temperature co-fired ceramic (LTCC) application. To check the performance of the prepared LTCC as substrate, a microstrip-fed aperture-coupled dual segment cylindrical dielectric resonator antenna (DS-CDRA) is designed using LMAP (x = 0.02) ceramic as substrate material and Barium Strontium Titanate with 10 wt% of PbO-BaO-B_2O_3-SiO_2 glass (BSTG) and Teflon as the components of resonating material. The simulation study of the DS-CDRA is performed using the Ansys High Frequency Structure Simulator (HFSS) software. A conductive coating of silver is used on the substrate. The simulated and measured −10 dB reflection coefficient bandwidths of 910 MHz (9.07–9.98 GHz at resonant frequency of 9.49 GHz) and 1080 MHz (8.68–9.76 GHz at resonant frequency of 9.36 GHz), respectively are achieved. The measured results of the fabricated antenna are found in good agreement with the simulation results. The prepared material can find potential applications in radar and radio navigation as well as radio astronomy and military satellite communication.

1. Introduction

Ceramic materials find application as substrates in integrated circuits, thermally stable resonators, filters, oscillators, phase shifters, isolators, circulators and dielectric resonator antennas in microwave and millimeter wave communication and radar systems. Low dielectric constant, low loss tangent and good thermal stability are primary requirements for substrate materials to achieve efficient signal transmission. Low loss ceramic materials used in the circuit improve its overall quality factor by reducing the power dissipation and the insertion loss, which suppresses the electrical noise in oscillators and can produce highly selective filters, low loss phase shifters and non-reciprocal devices [1]. Further, by selecting a low loss ceramic material for realizing a dielectric resonator antenna (DRA), the radiation efficiency can be enhanced due to low conductor and dielectric losses as well as absence of surface waves associated with DRA. Different manufacturers produce similar components for specific applications, however, there are subtle differences in their circuit designs, construction and packaging.

The material requirements for substrate applications are: low dielectric constant (ε_r < 20), Qf > 1000, low temperature variation of dielectric constant (Tk), high thermal conductivity, preferably low thermal expansion, chemical compatibility with the electrode material. Low sintering temperatures <950 °C with good densification are required to avoid melting metallic conductors like silver or gold in the fabrication of ceramic devices. Low temperature co-fired ceramics (LTCC) technology enables the fabrication of three dimensional ceramic modules with embedded silver or gold electrodes [2].

There are many ceramic materials with excellent microwave dielectric properties. However, these materials generally have high sintering temperatures [2]. Low sintering temperature is required for co-firing the ceramic with the electrode material e.g. silver or copper. In recent years, many researchers have found various materials with low sintering temperature (<1000 °C) and matching coefficient of thermal expansion with other co-firing materials for integration with miniaturized microwave

* Corresponding author. Department of Ceramic Engineering, Indian Institute of Technology (Banaras Hindu University), Varanasi, 221005, India. Tel.: +91 9621405467 (mobile).
E-mail address: preetikumari5501@gmail.com (P. Kumari).

https://doi.org/10.1016/j.jpcs.2017.10.028
Received 20 June 2017; Received in revised form 13 August 2017; Accepted 19 October 2017
Available online 21 October 2017
0022-3697/

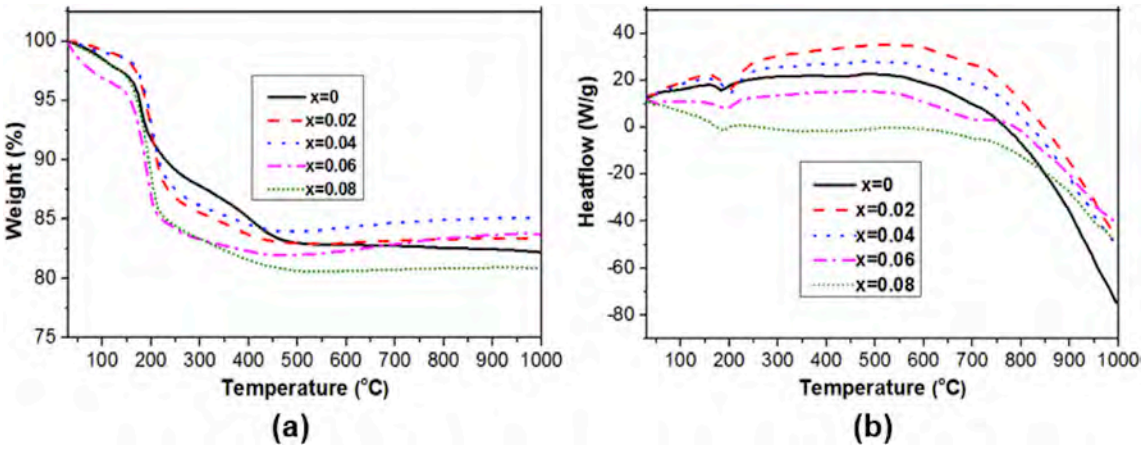

Fig. 1. (a) TG plot and (b) DTA plot of LMAP ceramics.

devices [3]. Also, only a handful of ultra-low temperature co-fired ceramic (ULTTC) materials with sintering temperatures less than 700 °C are developed [4–7]. Recently, Sebastian et al. reported a broad review on the current status of the LTCC [1,2] and ULTCC [8] materials developed so far.

To lower the sintering temperature, generally glass with low softening temperature is added to the ceramic systems. However, the addition of glass increases the loss tangent of the composite due to presence of network formers in the glasses. The microwave energy is possibly absorbed by the network formers [8]. There are two approaches to develop glass based LTCC materials i.e. glass-ceramic and glass + ceramic routes. The densification is achieved through controlled crystallization in glass ceramics [1,2,9]and liquid phase sintering in glass + ceramic routes [10–13] respectively. The commercially available LTCC materials are generally glass-ceramic or glass + ceramic materials. Recently, emphasis is given for the development of glass free ceramic systems to achieve good microwave dielectric properties with low loss and a small number of investigations has been reported for glass free ceramic systems with low sintering temperature [4,6,14–20].

The $LiMgPO_4$ ceramic system has been reported previously as a suitable LTCC material. Many researchers have studied this system by replacing Mg^{2+} with various transition metal elements like Zn, Cu, Ni, Co in different proportions [17–19,21,22]. Investigations on $LiMg_{(1-x)}A_xPO_4$ ceramic (with A = Zn^{+2}, Co^{+2}, Ni^{+2}) shows good microwave dielectric properties and chemical compatibility with electrode material silver. Dong et al. [23]. have studied $Ba_3(VO_4)_2$-$LiMgPO_4$ composite ceramics with good microwave dielectric properties and low sinterability temperature down to 850 °C.

Low sintering temperature material with good microwave dielectric properties can be utilized for microwave device applications like filters, couplers, diplexers, microstrip antennas and dielectric resonator antennas [24–30]. We believe that utilizing the prepared material is a viable approach for substrate application in microwave devices.

Initial part of this paper focuses on the study of the effect of Al_2O_3 addition in Li_2O-(2-3x)MgO-(x)Al_2O_3-P_2O_5 (LMAP) ceramics on their structural and dielectric properties. It is also important to study the design and development of microwave components and DRAs using LTCC substrates. Therefore, the second part of paper describes the study of a DS-CDRA designed using the prepared LMAP (x = 0.02) LTCC ceramic material. The simulation study on the proposed antenna was performed using Ansys HFSS software [31] and the simulation results for the DS-CDRA are compared with the respective measured results.

2. Experiments

2.1. Material synthesis and characterisation techniques

A series of samples having formula in Li_2O-(2-3x)MgO-(x)Al_2O_3-P_2O_5(LMAP), where x = 0, x = 0.02, x = 0.04, x = 0.06 and x = 0.08, were synthesized by conventional solid state route. High purity Li_2CO_3 (99%, Sigma Aldrich), MgO (99%, Sigma-Aldrich), Al_2O_3 (99.5%, Sigma Aldrich) and $NH_4H_2PO_4$ (99%, Alfa Aesar) were used as starting raw materials. Stoichiometric amount of raw materials were mixed thoroughly in ethanol medium for 8 h at 300 rpm using a Fritsch Planetary mill (Pulverisette 5/4). The ball milled batches were dried in oven at 50 °C for 16 h. Thermal reaction and decomposition behaviour of different batch compositions were studied using a Mettler Toledo (STAR system) TGA/DTA machine within the temperature range 30–1000 °C using a heating rate of 5 °C/min in argon atmosphere. The mixed powders were primarily calcined in air at 500 °C for 4 h followed by second calcination at 800 °C for 4 h with intermediate grinding. Calcined powder was ground into fine powder. Powder X-Ray diffraction patterns of the calcined sample were recorded using Rigaku X-ray diffraction with Cu K-Alpha radiation employing a Ni filter with scan rate of 2° per minute. The powders were pressed uniaxially to form cylindrical (diameter = 12 mm, thickness = 2 mm) and rectangular (length = 23 mm, width = 11 mm, height = 2–3 mm) pellets applying a load of 15 MPa. All pellets were sintered in the temperature range 825–925 °C with the heating and cooling rate of 2 °C per minute. The bulk density, water absorption and apparent porosity of the sintered pellets were determined by Archimedes principle. Maximum densification occurs at 825 °C for the LMAP samples with x = 0.02 to 0.08. For the pure sample (x = 0), the densification increases with the increase in sintering temperature up to 925 °C. It was also reported in the previous study that the maximum density for $LiMgPO_4$ ceramic is achieved at 950 °C and above this temperature; the densification decreases further [17]. All the pellets were sintered at optimized sintering temperature of 825 °C for 6 h. The surface morphology and energy dispersive spectra of all the sintered samples were carried out using Scanning Electron Microscope (ZEISS Instruments). High frequency dielectric measurements were carried out through transmission/reflection method within the frequency range 8.2–12.4 GHz using ENA E5071C Keysight Technologies make Network Analyser.

For the fabrication of DS-CDRA, Barium Strontium Titanate (BST) with 10 wt% of PbO-BaO-B_2O_3-SiO_2 glass (BSTG) [32] and teflon were used as the components of resonating material. The square substrate of LMAP (x = 0.02) ceramic having dimensions 42 mm × 42 mm × 1.5 mm was prepared by uniaxially pressing the calcined powder under hydraulic press. After sintering at 825 °C for 6 h, the obtained substrate is polished and made to the dimension of 40 mm × 40 mm × 1.2 mm.

2.2. Design of antenna on LTCC substrate

In order to check the suitability of the prepared material for application in microwave devices, a DS-CDRA antenna was designed and

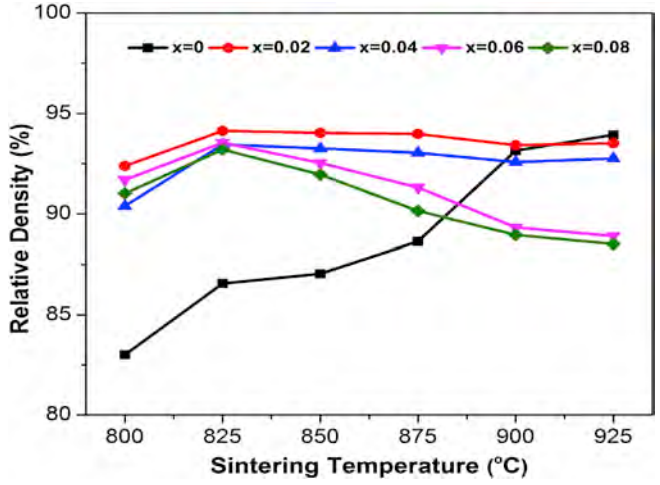

Fig. 2. Variation of percent relative density of LMAP ceramics at different sintering temperatures.

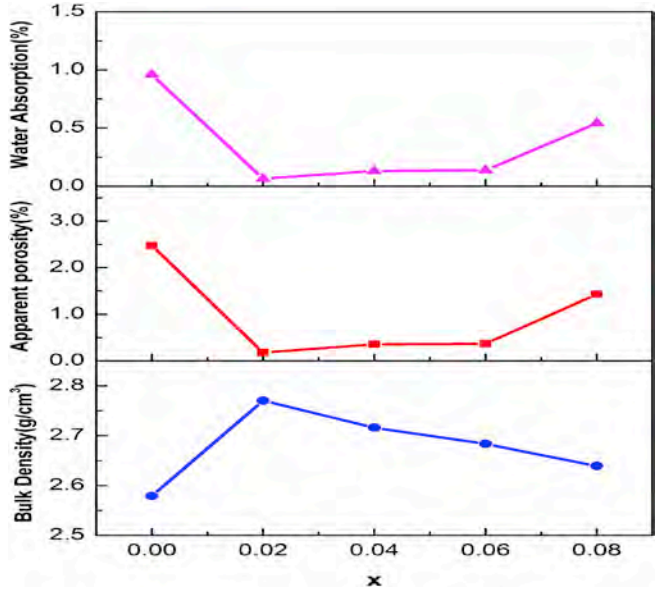

Fig. 3. Graphs of bulk density, percent apparent porosity and percent water absorption of LMAP ceramic with varying x content.

fabricated on single layer of LTCC substrate made from the low loss LMAP (x = 0.02) material. The antenna was designed using HFSS software and the parametric study was performed in order to optimize the dimensions of the DS-CDRA. The simulation results for the antenna parameters are compared with the respective measured results.

The CDRA is characterized by its height, radius and material dielectric constant. The LMAP (with x = 0.02) ceramic having maximum density when compared with the other compositions at low temperature of 825 °C is used as a substrate material with $\varepsilon_r = 6.2$ and $\tan\delta = 0.0006$. Silver coating was done on the substrate for making the conductive ground plane and the microstrip line for excitation of antenna through slot coupling. Silver coated substrate was first heated in oven for drying and then maturing of silver was done at 500 °C for 10 min. The upper segment of the proposed CDRA is made of high dielectric constant ceramic material (BSTG with $\varepsilon_r = 27$ and $\tan\delta = 0.121$) [32] and the lower segment is of low dielectric constant material (Teflon with $\varepsilon_r = 2.1$ and $\tan\delta = 0.001$).

3. Results and discussion

3.1. 1Analysis of material properties

3.1.1. TGA /DTA analysis

Thermo-gravimetric (TG) and Differential thermal analysis (DTA) of LMAP ceramics were done with heating rate of 5 °C/min. Fig. 1(a) and (b) show respectively the TGA and DTA of all samples. In Fig. 1(b), an endothermic peak is observed at 200 °C indicating the decomposition of lithium carbonate. Initially, a rapid weight loss of about 13% was observed up to 200 °C followed by weight loss of 15–18% up to 450 °C (Fig. 2(a)). The decomposition of lithium carbonate occurs at 157 °C [33], and the melting point of ammonium orthophosphate is 190 °C [34] after which its decomposition starts. Thus, the major weight loss observed up to 200 °C is due to decomposition of ammonium orthophosphate and carbonate, which produces ammonia and carbon dioxide.

The burnout process is completed at 450 °C. Total weight loss of about 18% was observed within the temperature range 30–450 °C. There was no further weight loss above 450 °C in the TG curve. It may be associated with the solid reaction process forming the crystal phase of $LiMgPO_4$ [33]. Thus, the primary calcination temperature is taken as 500 °C followed by second calcination at 800 °C for 4 h. Second calcination was done because there is a possibility of lithium escape at higher temperature. So, if the compound is formed, this escape can be decreased. Moreover, double calcination makes the powder more homogeneous.

Addition of Al_2O_3 affects the thermal behaviour of these ceramic compositions. It can be seen from the DTA/TG plots that with initial addition of Al_2O_3, the reactivity between the constituent materials increases. It reflects in faster decomposition of Li_2CO_3 at lower temperatures. With addition of Al_2O_3 more than x = 0.04, the reaction temperature increases again.

3.1.2. Sintering and densification behaviour

Pellets of different batches were sintered at different temperatures ranging from 800 to 925 °C for 6 h. The plot of percent relative density with sintering temperature is given in Fig. 2. At 800 °C, with the addition of small amount of Al_2O_3 (x = 0.02), an increase in the relative density by around 9% (from 83.00 to 92.39%) is observed. When the densification behaviour is seen at different sintering temperatures, maximum density is achieved at the sintering temperature of 825 °C for the different compositions (x = 0.02–0.08). Maximum relative density of 94.13% is achieved for the composition with x = 0.02 at the sintering temperature of 825 °C. For the LMP (x = 0) sample, the densification increases with increase in sintering temperature. It is also reported by Dong et al. that pure $LiMgPO_4$ ceramic attains its maximum relative density at 950 °C, which is around 95% of the theoretical density [22].

Thus, the optimized sintering temperature is 825 °C and all the investigations and material characterizations were performed for the samples sintered at this temperature.

The plots of bulk density, percent apparent porosity and water absorption are shown in Fig. 3. The water absorption, apparent porosity and bulk density were calculated by using the following relation [35]:

$$\text{Water absorption } (\%) = \frac{W - D}{D} \times 100$$

$$\text{Apparent porosity } (\%) = \frac{W - D}{W - S} \times 100$$

$$\text{Bulk density } \left(\text{g.cm}^{-3}\right) = \frac{D}{W - S}$$

where, D is the dry weight of test sample, W is the saturated weight or soaked weight and S is the suspended weight in water after boiling for 2 h and then cooled test sample. The maximum bulk density of 2.77 and

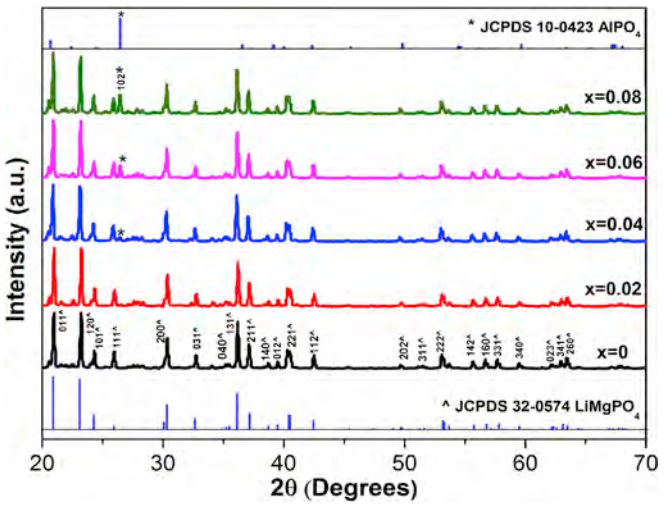

Fig. 4. XRD patterns of LMAP ceramics.

minimum apparent porosity of 0.18% were observed in case of composition with x = 0.02. There is a significant decrease in apparent porosity when Al_2O_3 is introduced. Apparent porosity corresponds to the volume of the open pores to its exterior volume [35]. The composition with x = 0 does not densify properly at 825 °C showing maximum apparent porosity of 2.47% but for the composition with x = 0.02, density increases and the percent apparent porosity decreases to 0.18%. Beyond x = 0.02, the values of apparent porosity are in the range 0.36–1.43%. Thus, it can be concluded from the above discussion that the addition of small amount of Al_2O_3 (x = 0.02) improves the densification at lower sintering temperature of 825 °C.

3.1.3. Crystal structure

Fig. 4 illustrates the X-ray diffraction patterns of Li_2O-(2-3x)MgO-(x) Al_2O_3-P_2O_5(x = 0–0.08) ceramics sintered at 825 °C for 6 h. Since optimized sintering temperature is 825 °C therefore it can be useful for LTCC application. All samples show an orthorhombic olivine type phase of $LiMgPO_4$ (JCPDS file no. 32-0574) along with $AlPO_4$ as a minor phase (JCPDS file no. 10-0423). $AlPO_4$ (α-Berlinite) possesses a hexagonal structure (JCPDS file no. 10-0423) [36]. The diffraction peaks of $LiMgPO_4$ are indexed for composition x = 0 in Fig. 4. Peak due to basic $LiMgPO_4$ are common in all the compositions up to x = 0.08. A diffraction peak due to the maximum intensity of secondary $AlPO_4$ has been observed in composition x = 0.04 to 0.08 beside the common peaks of $LiMgPO_4$ and indexed. When x concentration increases from 0.02 to 0.08, the intensity of $AlPO_4$ peak increases and diphasic composite of $LiMgPO_4$ and $AlPO_4$ forms. It may be due to the large difference in the ionic radii of Al^{3+} and Mg^{2+}. The different crystal structures of $LiMgPO_4$ and $AlPO_4$ having different linkages of polyhedral units and the different valencies of Al^{3+} and Mg^{2+} limit the formation of solid solutions between $LiMgPO_4$ and $AlPO_4$.

3.1.4. Microstructure

Fig. 5 shows the SEM microstructure of all samples at magnification of 5 K. The SEM micrograph of the composition with x = 0 (Fig. 5 (a)), shows lower densification on sintering at 825 °C. Addition of small amount of Al_2O_3 (x = 0.02–0.04) results in the bimodal grain distribution as shown in Fig. 5(b) and (c). As a result of this bimodal grain distribution, the density has increased. But, by further increasing its content (x > 0.06), it results in exaggerated grain growth of some $LiMgPO_4$ crystal, which results in higher porosity in the specimen. The oversized grain can be clearly seen in Fig. 5(d) and (e). The presence of secondary $AlPO_4$ crystal in the ceramic matrix, marked in Fig. 5(e), is clearly visible for the LMAP (x = 0.08) sample. The SEM micrograph of LMAP (x = 0.02) ceramic with 20 wt% Ag is shown in Fig. 5(f). It confirms that silver is not reacting with the prepared ceramic and thus, it can be utilised as the electrode material in device applications.

In Fig. 6, EDS analysis and mapping of Al, P, O and Mg ions in the LMAP (x = 0.08) is shown. Fig. 6(a) shows the SEM microstructure of LMAP composition with x = 0.08 at magnification of 10 K. Lithium, being the light element does not get detected in the EDS spectrum while the presence of magnesium, phosphorus, aluminium and oxygen is visible in the EDS spectrum (Fig. 6(b)). The elemental mapping of oxygen and phosphorus is homogeneous at all the places in the sample as shown in Fig. 6(c) and (d) respectively. In $AlPO_4$, magnesium is absent and in $LiMgPO_4$, aluminium is absent. So, when the elemental distribution of aluminium and magnesium are recorded as in Fig. 6(e) and (f) respectively, elemental mapping shows the absence of magnesium where small crystallites of $AlPO_4$ are visible. The presence of $AlPO_4$ in the ceramic matrix is confirmed by XRD, but the $AlPO_4$ crystallites are not very clearly seen at lower x values (up to 0.06) in SEM micrographs. It is clearly seen in Fig. 6(a) that a chain or cluster of $AlPO_4$ crystals (1–2 μm) form along with the large $LiMgPO_4$ grains in LMAP (x = 0.08) ceramics. Thus, it can be concluded that small addition of Al_2O_3 (x = 0.02–0.04), enhances the density of the ceramic matrix because of the partial

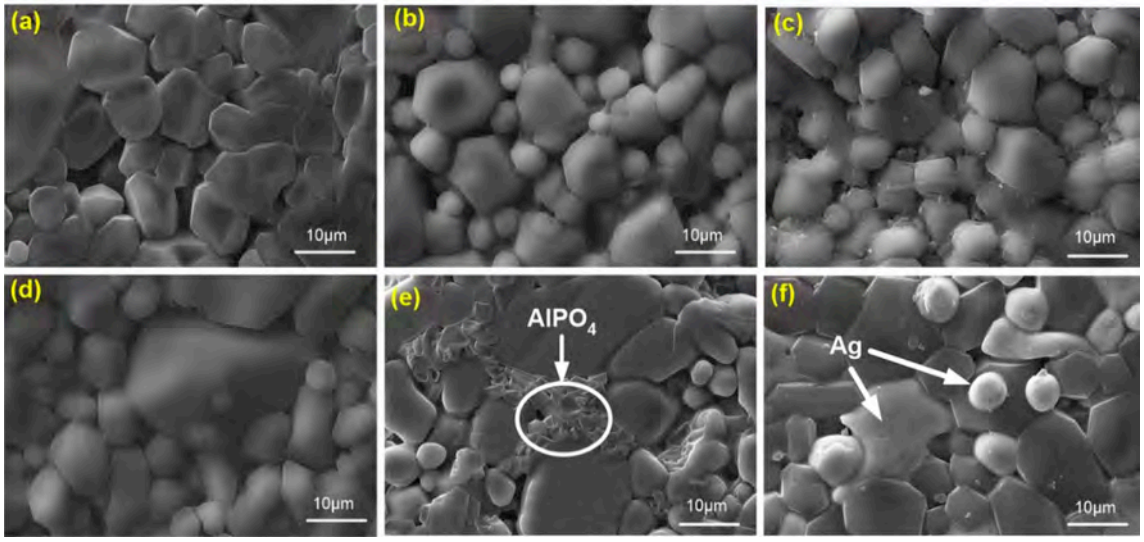

Fig. 5. The SEM microstructure of LMAP ceramics (a) x = 0, (b) x = 0.02, (c) x = 0.04, (d) x = 0.06, (e) x = 0.08 and, (f) back scattered image of LMAP (x = 0.02) with 20 wt% Ag.

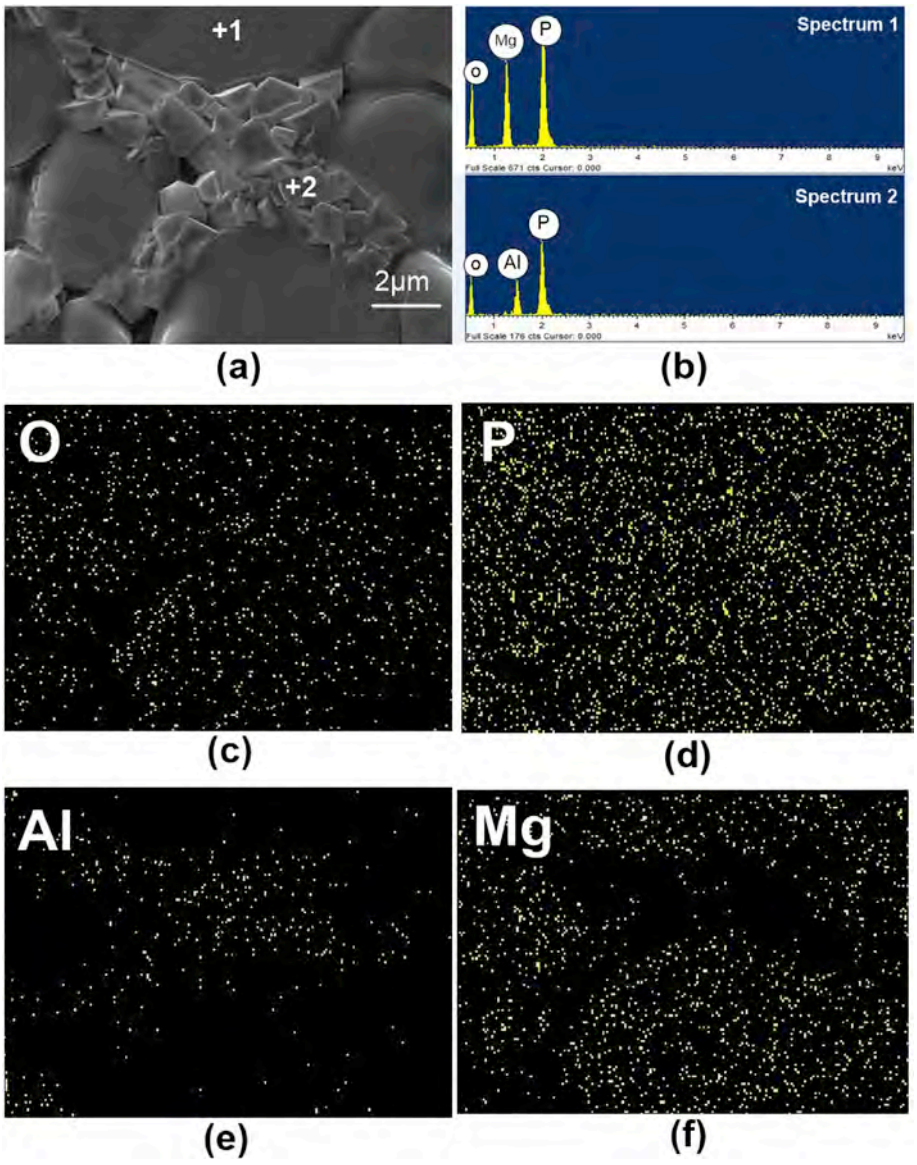

Fig. 6. SEM/EDS spectra and elemental mapping of Li_2O-(1.76)MgO-(0.08)Al_2O_3-P_2O_5ceramics sintered at 825 °C, showing the presence of $AlPO_4$ crystals.

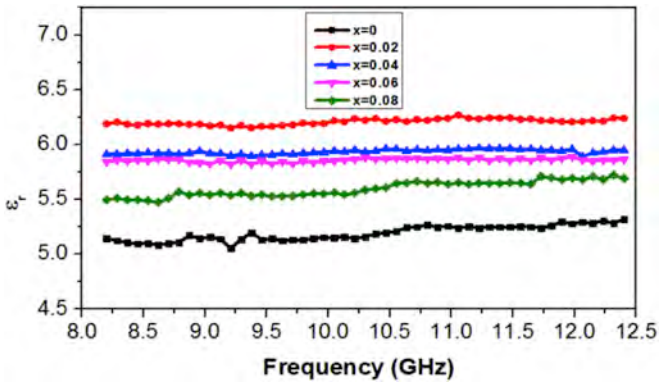

Fig. 7. The variation of relative permittivity ε_r of LMAP ceramics with frequency.

dissolution of Al_2O_3 in the matrix. Further increase in Al_2O_3 content (x = 0.06–0.08) results in exaggerated grain growth and also formation of secondary $AlPO_4$ phase.

3.1.5. *Dielectric characterization*

There is a direct correlation of dielectric constant values with the density of the material. If the density is higher, the dielectric constant values will also be higher. Therefore, the dielectric constant of around 5 is observed for the LMP (x = 0) ceramic sintered at 825 °C, which consists

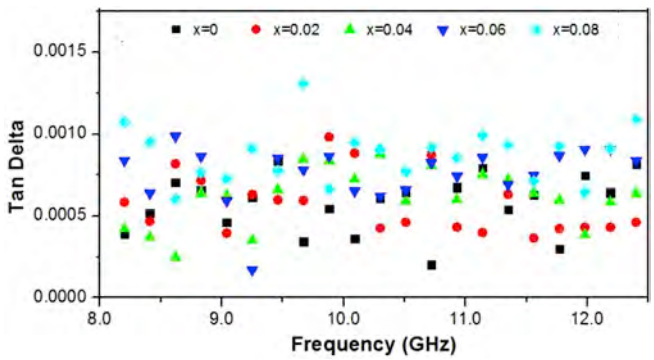

Fig. 8. Tan delta variation for different LMAP compositions with frequency.

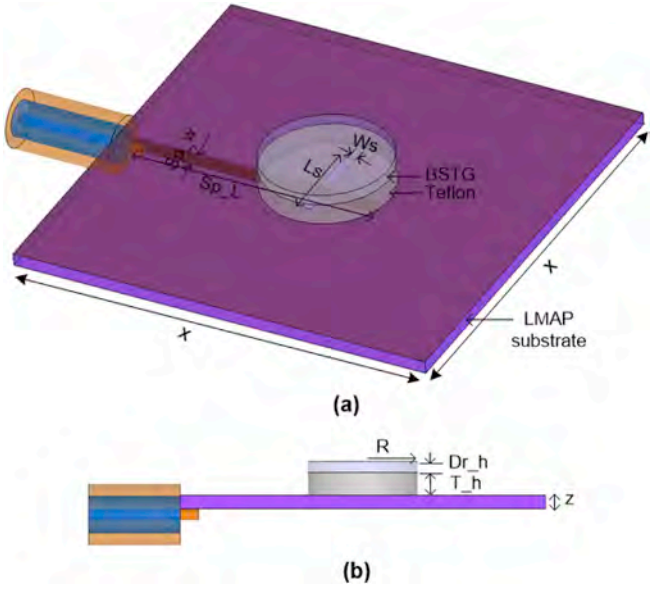

Fig. 9. Geometry of proposed antenna (a) 3-D view and (b) side view.

of single $LiMgPO_4$ phase. Had it been sintered at 925 °C or above, it would have shown higher densification and greater dielectric constant (>6) [19,22]. But in case of composition with x = 0.06 to 0.08, the dielectric constant value decreases due to the formation of low dielectric constant $AlPO_4$ and increased porosity. The $AlPO_4$-5 wt% MgF_2 composite sintered at 1450 °C shows good microwave dielectric properties (ε_r = 3.0 and loss tangent = 7×10^{-3}) [2,37]. The values of ε_r for different ceramic compositions lie within the range 5.0–6.2 (Fig. 7). It is to be noted that the value of ε_r for LMAP ceramic having x = 0.02 is found to be 6.2.

The loss tangent values of these ceramic compositions lie in the order of 10^{-4} in X-Band (Fig. 8). Again it is worthwhile to mention here that LMAP ceramic has loss tangent of 0.0006 for x = 0.02. The materials with low ε_r and low-loss find several applications in microwave engineering for reduction in RC signal delay and are in constant demand. Low relative permittivity also decreases power consumption and reduces cross-talk [1]. Optimisation in permittivity can be achieved through the control of density by addition of Al_2O_3 in the LMAP ceramics, keeping in mind that the device must possess good mechanical, chemical and thermal stability. The LMAP ceramic show good dielectric properties in X-Band of microwave frequencies.

3.2. Design and analysis of DS-CDRA

3.2.1. Antenna design

The geometry of the proposed antenna is shown in Fig. 9. The LMAP (x = 0.02) ceramic (ε_r = 6.2 and tanδ = 0.0006) having dimensions 40 mm × 40 mm × 1.2 mm is taken as substrate (Fig. 10(a)). The top surface of the substrate is silver coated, acting as a conducting ground plane. An aperture (slot) of length 8 mm and width 0.9 mm was etched in the conducting ground plane at the centre on the top of the substrate as shown in Fig. 10(b). The antenna structure having two dielectric cylindrical segments is placed in the central region of the conducting ground plane above the aperture as shown in Fig. 9(a). The stacking of the two cylindrical dielectric segments, each having 12 mm of diameter, is done as shown in Fig. 9(b). The heights of the lower segment (made of Teflon having ε_r = 2.1 and tanδ = 0.001) and the upper segment (made of BSTG having ε_r = 27 and tanδ = 0.121) is 2 mm and 1 mm, respectively. The active pattern corresponding to the 50Ω microstrip feedline of length 25 mm and width 1.6 mm, is printed at the bottom side of the substrate, perpendicular to the length (or larger dimension) of the slot as shown in Fig. 9(a). To excite the DS-CDRA, aperture coupling was used. The size of the aperture (slot) and extension of microstrip line beyond the slot which is about one quarter guide wavelength were optimized through simulation. All the optimized antenna parameters are given in Table 1. Aperture coupling prevents the slot from the spurious feed radiation since the slot gets isolated from the microstrip feed network located below the ground plane. The most common method for exciting the CDRA is the probe or coaxial feed method. However, aperture coupling is selected in order to get the advantage of less spurious feed radiation, large bandwidth and ease of fabrication [29]. The top and bottom views of the fabricated prototype are shown in Fig. 10(c) and (d), respectively.

Table 1
Optimized antenna parameters of proposed DS-CDRA.

Parameters	Dimensions (mm)	Parameters	Dimensions (mm)
Substrate length, x	40	Stripline width, Sp_w	1.6
Substrate thickness, z	1.2	Stripline length, Sp_L	25
Slot length, Ls	8	BSTG height, Dr_h	1
Slot width, Ws	0.9	Teflon height, T_h	2
Radius, R	6		

The simulation study of a DS-CDRA designed on LMAP (x = 0.02) LTCC ceramic substrate for X-band application is described. The simulation study was performed using Ansys HFSS software.

3.2.2. Reflection coefficient-frequency characteristics

From the simulation results, it was observed that the −10 dB reflection coefficient bandwidth of 910 MHz (9.07–9.98 GHz) is achieved with resonant frequency of 9.49 GHz for optimized slot size. The reflection coefficient – frequency characteristics of the proposed DS-CDRA for different slot size were simulated and the results are shown in Fig. 11(a). It can be observed from Fig. 11(a) that as the slot length increases, the resonant frequency decreases. The optimized slot length 'Ls' and width

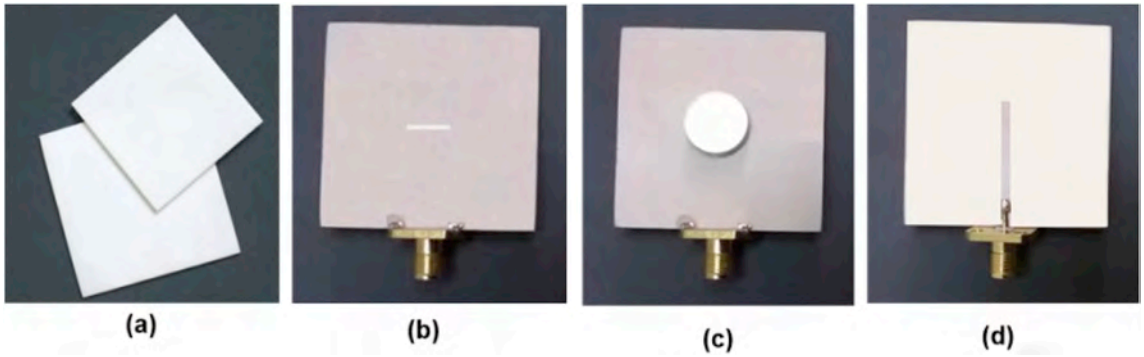

Fig. 10. (a) Substrate image, (b) slot on fabricated antenna, (c) top view and, (d) bottom view of the fabricated antenna.

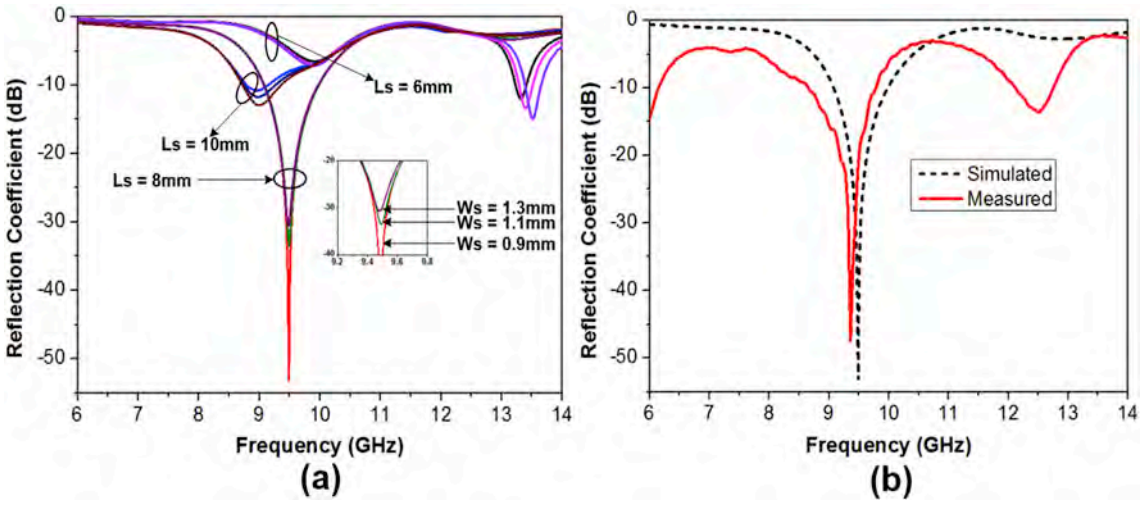

Fig. 11. (a) Simulated reflection coefficient–frequency plots of the proposed DS-CDRA for different slot length and width combinations; (b) Simulated and measured reflection coefficient–frequency plots of the proposed DS-CDRA for optimized slot dimensions.

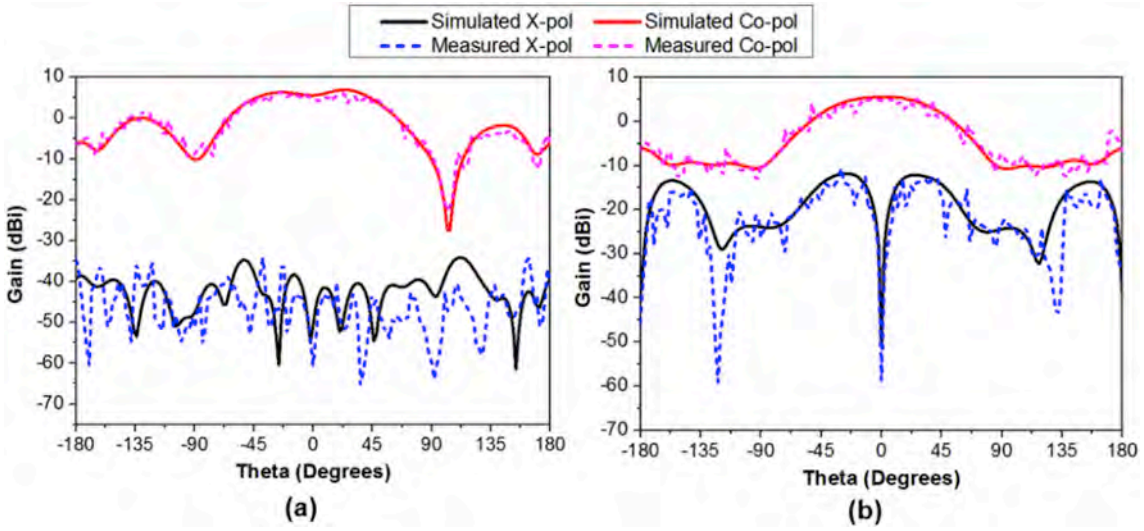

Fig. 12. Simulated and measured radiation patterns of proposed DS-dual segment CDRA at 9.36 GHz **(a)** H-plane (co and x-polar) radiation patterns; **(b)** E-plane (co and x-polar) radiation patterns.

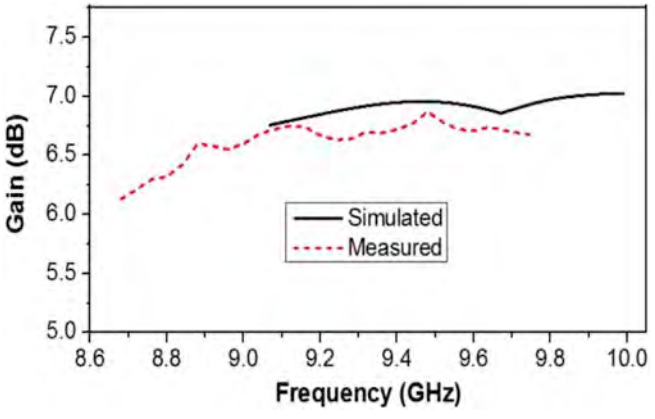

Fig. 13. Simulated and measured gain-frequency plot of proposed DS-CDRA.

'Ws' are found to be 0.8 mm and 0.9 mm respectively, corresponding to minimum input reflection coefficient value of −53 dB at the resonant frequency of 9.49 GHz.

The reflection coefficient–frequency characteristics of the fabricated antenna of the optimized dimensions were measured and the

Table 2
Radiation pattern characteristics of DS-CDRA at 9.36 GHz.

Parameters		Simulated	Measured
−3 dB beam width (degrees)	E-plane	130°	134°
	H-plane	146°	144°
Front-to-back ratio (dB)	E-plane	11.73	11.64
	H-plane	12.76	10.78

Table 3
Highest cross-polarised lobe level with corresponding angle at 9.36 GHz for DS-CDRA.

Parameters		Simulated	Measured
E-plane	Highest cross polar level (dB)	−11.81	−10.58
	Angle (degree)	−26°	−30°
H-plane	Highest cross polar level (dB)	−34.14	−34.29
	Angle (degree)	112°	−38°

Table 4
Comparison of different stacked dielectric resonator antenna operating at different frequencies.

DRA shape	ε_r	ε_s	Resonant frequency(GHz)	Excitation	Peak Gain	Physical Dimensions		Percent Bandwidth	Ref.
						a(mm)	h(mm)		
Stacked CDRA	6.15	3.4	5.8	Aperture	11.6dBi	44.1	22.75	2.6	[38]
Stacked RDRA	2.1/27	4.2	9.1	Aperture	6.63 dB	10 × 8	4.1	7.5	[32]
Proposed DS-CDRA	2.1/27	6.2	9.36	Aperture	6.87 dB	12	3	11.71	–

εr and εs: permittivity of DRA material and substrate; a: diameter for cylindrical DRA, ˆ: Length and width of rectangular DRA; h: height of DRA.

measurement results are shown in Fig. 11(b). It can be observed from Fig. 11(b) that measured input characteristics of the proposed antenna is nearly in agreement with the simulated characteristic. The measured −10 dB reflection coefficient bandwidth of the proposed antenna is found to be 1080 MHz (8.68–9.76 GHz) with resonant frequency of 9.36 GHz.

3.2.3. Radiation patterns and gain

The co- and cross-polar radiation patterns (2D) of the proposed antenna in E- and H-plane at 9.36 GHz are shown in Fig. 12, whereas realized gain-frequency characteristics of the antenna are shown in Fig. 13. It is observed from Fig. 12 that E- and H-plane beamwidths lie in the range 124 - 154° and 138 - 146°, respectively at the frequency of interest (see Table 2). The broadside radiation patterns are achieved in both E- and H- planes over the operating bandwidth of the antenna with fairly low cross-polarized levels in E-plane. The highest cross-polarized lobe levels with corresponding angles of the antenna in E- and H-planes for different frequencies extracted from Fig. 12 are given in Table 3. The simulated and measured peak gain values are found to be 6.96 and 6.69 dB at frequencies of 9.49 and 9.36 GHz respectively.

Co- and cross-polar radiation patterns of fabricated DS-CDRA in far field region were measured in anechoic chamber at 9.36 GHz, where a horn antenna was used as transmitting antenna and the proposed DS-CDRA was positioned in the far field region at receiving end. It is observed from Fig. 12 that simulated radiation patterns of the antenna in both E- & H-planes are similar to the respective measured patterns. The deviation in the simulation and measured results may be due to human and fabrication errors.

From these results, it can be concluded that the designed antenna on the LTCC substrate material provides good impedance bandwidth and gain, without hampering the antenna performance. Thus, it can be used to design and develop an antenna providing reasonable bandwidth and gain. Further, it can be said that low loss LTCC material can be used to design electronic devices such as filters and phase shifters having improved characteristics.

Many studies on dielectric resonator antennas (DRAs) using different ε_r values of resonator material have been reported at different frequencies [26]. Mrnka et al. [38] reported a stacked cylindrical DRA in which resonating element is made by stacking of 14 layers of resonator material with ε_r value of 6.15. Its overall dimensions and other details is given in Table 4. It pertains to stacked CDRA but the study was done in C-Band. Their percent impedance bandwidth is much lower than the proposed one [see Table 4]. Another study on stacked rectangular DRA (RDRA) [32] with similar stacking as in proposed DS-CDRA, has also been reported. Its operating frequency range lies in the same band, i.e. X-Band. The percent impedance bandwidth of stacked RDRA reported in literature is lower than the proposed stacked antenna [Table 4]. The proposed DS-CDRA provides wide impedance bandwidth of 11.7% with reasonably good gain of 6.87 dB for X-Band application.

4. Conclusions

In the present work, the LMAP ceramic has been found to have good structural and microwave dielectric characteristics. From the XRD analysis, it has been observed that LMAP ceramic forms a dibasic composite of $LiMgPO_4$ and $AlPO_4$. The small addition of Al_2O_3 in LMAP ceramic decreases the sintering temperature from 950 °C to 825 °C. The $AlPO_4$ crystallites have been observed in case of ceramic composition with x = 0.08. Dielectric constant for LMAP ceramics with different values of x lies in the range 5.0–6.2 in X-band (8.2–12.4 GHz).

Further, the LMAP ceramic (x = 0.02) has been used as LTCC substrate for simulation and experimental studies of DS-CDRA. The simulation and experimental results show the favourable radiation patterns. It can be inferred from these results that broadside radiation patterns are obtained in both E- and H-planes at the resonant frequency of the antenna with fairly low cross polar levels in E-plane. The measured results of the fabricated DS-CDRA have been found to be nearly in agreement with corresponding simulation results. The simulated and measured values of gain lie in the ranges 6.76–7.02 dB and 6.13–6.87 dB respectively over the operating bandwidth of antenna. The proposed antenna can find application in microwave communication, radar and communication systems.

It is concluded that the proposed material can be used as LTCC substrate material in realization of low loss microwave components and dielectric resonator antennas for radar, radio navigation, radio astronomy and satellite communication.

References

[1] M.T. Sebastian, H. Jantunen, Low loss dielectric materials for LTCC applications: a review, Int. Mater. Rev. 53 (2) (2015) 57–90, https://doi.org/10.1179/174328008X277524.

[2] M.T. Sebastian, R. Ubic, H. Jantunen, Full critical review: low loss dielectric ceramic materials and their properties, Int. Mater. Rev. 60 (7) (2015) 392–412, https://doi.org/10.1179/1743280415Y.0000000007.

[3] D. Thomas, P. Abhilash, M.T. Sebastian, Casting and characterisation of $LiMgPO_4$ glass free LTCC tape for microwave application, J. Eur. Ceram. Soc. 33 (2013) 87–93, https://doi.org/10.1016/j.jeurceramsoc.2012.08.002.

[4] N. Joseph, J. Varghese, T. Siponkoski, M. Teirikangas, M.T. Sebastian, H. Jantunen, Glass-free $CuMoO_4$ ceramic with excellent dielectric and thermal properties for ultralow temperature cofired ceramic applications, ACS Sustain. Chem. Eng. 4 (2016) 5632–5639, https://doi.org/10.1021/acssuschemeng.6b01537.

[5] J. Varghese, T. Siponkoski, M. Teirikangas, M.T. Sebastian, A. Uusimaki, H. Jantunen, Structural, dielectric, and thermal properties of Pb free molybdate based ultra low temperature glass, ACS Sustain. Chem. Eng. 4 (2016) 3897–3904, https://doi.org/10.1021/acssuschemeng.6b00721.

[6] E.K. Suresh, K. Prasad, N.S. Arun, R. Ratheesh, Synthesis and microwave dielectric properties of A16V18O61 (a = Ba, Sr and Ca) ceramics for LTCC applications, J. Electron. Mater. 45 (6) (2016) 2996–3002, https://doi.org/10.1007/s11664-016-4388-6.

[7] I.J. Induja, M.T. Sebastian, Microwave dielectric properties of $SnO\text{-}SnF_2\text{-}P_2O_5$ glass and its composite with alumina for ULTCC applications, J. Am. Ceram. Soc. (2017) 1–9, https://doi.org/10.1111/jace.14804.

[8] M.T. Sebastian, Hong Wang, Heli Jantunen, Low temperature co-fired ceramics with ultra-low sintering temperature: a review, Curr. Opin. Solid State Mater. S. C. 20 (2016) 151–170, https://doi.org/10.1016/j.cossms.2016.02.004.

[9] P. Kumari, P. Tripathi, O. Parkash, D. Kumar, Low temperature sintering and characterisation of $MgO\text{-}B_2O_3\text{-}SiO_2$ glass ceramics for LTCC substrate application, Trans. Ind. Ceram. Soc. 75 (4) (2016) 229–233.

[10] T.S. Sasikala, M.N. Suma, C. Pavithran, M.T. Sebastian, Forsterite-based ceramic glass composites for substrate applications in microwave and millimetre wave communications, J. Alloys Compd. 461 (2008) 555–559.

[11] K.M. Manu, P.S. Anjana, M.T. Sebastian, Low permittivity $SrCuSi_4O_{10}$-LMZBS glass composite for LTCC applications, Mater. Lett. 65 (2011) 565–567.

[12] J. Varghese, S. Gopinath, M.T. Sebastian, Effect of glass fillers in Cu2ZnNb2O8 ceramics for advanced microwave applications, Mater. Chem. Phys. 137 (2013) 811–815.

[13] S. Arun, M.T. Sebastian, K.P. Surendran, $Li_2ZnTi_3O_8$ based high k LTCC tapes for improved thermal management in hybrid circuit applications, Ceram. Int. 43 (7) (2017) 5509–5516, https://doi.org/10.1016/j.ceramint.2017.01.073.

[14] J.J. Bian, J.Y. Wu, Designing of glass-free LTCC microwave ceramic- $Ca_{1-x}(Li_{0.5}Nd_{0.5})_xWO_4$ by crystal chemistry, J. Am. Ceram. Soc. 95 (1) (2012) 318–323, https://doi.org/10.1111/j.1551-2916.2011.04790.x.
[15] Jianjiang Bian, Yaomin Ding, A new glass-free LTCC microwave ceramic – (1-x) $Li_{2.08}TiO_3$ + xLiF, Mater. Res. Bull. 49 (2014) 245–249, https://doi.org/10.1016/j.materresbull.2013.08.076.
[16] Matjaz Valant, Danilo Suvorov, Glass-free low-temperature cofired ceramics: calcium germanates, silicates and tellurates, J. Eur. Ceram. Soc. 24 (2004) 1715–1719, https://doi.org/10.1016/S0955-2219(03)00483-7.
[17] D. Thomas, M.T. Sebastian, Temperature compensated $LiMgPO_4$: a new glass free low temperature glass free ceramic, J. Am. Ceram. Soc. 93 (2010) 3828–3831, https://doi.org/10.1111/j.1551-2916.2010.03934.x.
[18] D. Thomas, M.T. Sebastian, Effect of Zn^{2+}substitution on the microwave dielectric properties of $LiMgPO_4$ and the development of a new temperature stable glass free LTCC, J. Eur. Ceram. Soc. 32 (2012) 2359–2364, https://doi.org/10.1016/j.jeurceramsoc.2012.01.031.
[19] M.T. Sebastian, Dielectric Materials for Wireless Communication, Elsevier, Oxford, 2008.
[20] X. Chou, Z. Zhao, W. Zhang, J. Zhai, Microstructures and dielectric properties of $Ba_{0.5}Sr_{0.5}TiO_3$-Zn_2TiO_4 composite ceramics with low sintering temperature for tunable device applications, Mater. Des. 31 (2010) 3703–3707, https://doi.org/10.1016/j.matdes.2010.03.006.
[21] Z.W. Dong, Y. Zheng, P. Cheng, X.P. Lv, W.Y. Zhang, W. Zhou, W.H. Xiong, Preparation and microwave dielectric properties of $Li(Mg_{1-x}Co_x)PO_4$ ceramics for low temperature cofired ceramic applications, Ceram. Int. 40 (2014) 14865–14869, https://doi.org/10.1016/j.ceramint.2014.06.081.
[22] Z.W. Dong, Y. Zheng, P. Cheng, X.P. Lv, W. Zhou, Microwave dielectric properties of $Li(Mg_{1-x}Ni_x)PO_4$ ceramics for LTCC applications, Ceram. Int. 40 (2014) 12983–12988, https://doi.org/10.1016/j.ceramint.2014.04.160.
[23] Z.W. Dong, Y. Zheng, P. Cheng, X.P. Lv, W. Zhou, Microwave dielectric properties of low-temperature sinterable $Ba_3(VO_4)_2$-$LiMgPO_4$ composite ceramics, Mater. Lett. 131 (2014) 151–153, https://doi.org/10.1016/j.matlet.2014.05.144.
[24] U. Ullah, W.F.F. Wan Ali, M.F. Ain, N.M. Mahyuddin, Z.A. Ahmad, Design of a novel dielectric resonator antenna using $MgTiO_3$-$CoTiO_3$ for wideband applications, Mater. Des. 85 (2015) 396–403, https://doi.org/10.1016/jmatdes.2015.07.026.
[25] Reena Kumari, Ravi Kumar Gangwar, Circularly polarized dielectric resonator antennas: design and developments, Wirel. Pers. Commun. 86 (2016) 851–886, https://doi.org/10.1007/s11277-015-2959-0.
[26] J. Kumar, N. Gupta, Performance analysis of dielectric resonator antennas, Wirel. Pers. Commun. 75 (2) (2013) 1029–1049, https://doi.org/10.1007/s11277-013-1406-3.
[27] C.A. Balanis, Antenna Theory Third Edition, Analysis and Design, Wiley, New York, 2005.
[28] C. Menudier, M. Thevenot, L. Huitema, E. Arnaud, T. Monediere, O. Tantot, S. Bila, N. Delhote, Innovative materials and fabrication process to develop new RF components and concepts, in: 11th European Conference on Antennas and Propagation (EUCAP), 2017.
[29] A. Petosa, Dielectric Resonator Antennas Handbook, Artech House, London, 2007.
[30] K.M. Luk, K.W. Leung, Dielectric Resonator Antennas, Research Studies Press Ltd., Baldock, 2003.
[31] Ansoft Corporation. [Online] Available: http://www.ansoft.com.
[32] P. Tripathi, P. Kumari, B. Sahu, S.P. Singh, O. Parkash, D. Kumar, Design of rectangular dielectric resonator antenna using glass added barium Strontium titanate, in: International Conference on Microwave and Photonics (ICMAP), Dhanbad, India, Dec. 2015, pp. 11–13, https://doi.org/10.1109/ICMAP.2015.7408748.
[33] Mingming Shi, D. Zhang, C. Chang, Tunable emission and concentration quenching of Tb3+ in magnesium phosphate lithium, J. Alloys Compd. 627 (2015) 25–30, https://doi.org/10.1016/j.jallcom.2014.11.178.
[34] D.R. Lide, CRC Handbook of Chemistry and Physics 88th Edition 2007-2008, CRC Press, Taylor & Francis, Boca Raton, FL, 2007, pp. 4–46.
[35] ASTM C20–00 (Reapproved 2010), Standard test methods for apparent porosity, water absorption, apparent specific gravity, and bulk density of burned refractory brick and shapes by boiling water. [http://www.astm.org/standards/C20-00].
[36] Diane M. Christie, N. Troullier, James R. Chelikowsky, Electronic and structural properties of alpha-berlinite ($AlPO_4$), Solid state Commun. 98 (10) (1996) 923–926, https://doi.org/10.1016/0038-1098(96)00766-1.
[37] P. Abhilash, D. Thomas, M.T. Sebastian, Sintering and microwave dielectric properties of $AlPO_4$-MgF_2 ceramic composite, Int. J. Mod. Phys. 22 (2013) 159–163, https://doi.org/10.1142/S2010194513010052.
[38] Michal Mrnka, Zbynek Raida, Enhanced-gain dielectric resonator antenna based on the combination of higher-order modes, IEEE Antenna Wirel. Propag. Lett. 15 (2016) 710–713, https://doi.org/10.1109/LAWP.2015.2470099.